Title: Brain Angiopathy and Impaired Glucose Logistics in Mice with Psychosis-related Higher Brain Dysfunction

Short title: Angiopathy in mice and humans with psychosis

Authors: Shinobu Hirai[1,†], Hideki Miwa[1,2], Tomoko Tanaka[1], Kazuya Toriumi[3], Yasuto Kunii[4], Takuya Sakamoto[5], Mizuki Hino[4], Ryuta Izumi[4], Atsuko Nagaoka[4], Hirooki Yabe[4], Tomoya Nakamachi[6], Seiji Shioda[7], Takashi Dan[8], Toshio Miyata[8], Yasumasa Nishito[9], Hiroko Shimbo[1], Kazuhiro Suzuki[3], Mitsuhiro Miyashita[3], Masanari Itokawa[3], Makoto Arai[3], Haruo Okado[1,†]

Affiliations: [1]Neural Development Project, Department of Brain Development and Neural Regeneration, Tokyo Metropolitan Institute of Medical Science, Tokyo 156-8506, Japan.

[2]Molecular Neuropsychopharmacology Section, Department of Neuropsychopharmacology, National Institute of Mental Health, National Center of Neurology and Psychiatry, Tokyo 187-8553, Japan.

[3]Schizophrenia Research Project, Department of Psychiatry and Behavioral Sciences, Tokyo Metropolitan Institute of Medical Science, Tokyo 156-8506, Japan.

[4]Department of Neuropsychiatry, School of Medicine, Fukushima Medical University, Fukushima 960-1295, Japan.

[5]Department of Applied Biological Science, Faculty of Science and Technology, Tokyo University of Science, 2641 Yamazaki, Noda, Chiba 278-8510, Japan.

[6]Laboratory of Regulatory Biology, Graduate School of Science and, Engineering, University of Toyama, Toyama 930-8555, Japan.

[7]Global Research Center for Innovative Life Science, Peptide Drug Innovation, Hoshi University, Tokyo 142-8501, Japan.

[8]Division of Molecular Medicine and Therapy, Tohoku University Graduate School of Medicine, Miyagi 980-8575, Japan.

[9]Center for Basic Technology Research, Tokyo Metropolitan Institute of Medical Science, Tokyo 156-8506, Japan.

[†]These authors contributed equally to this work.

Correspondence should be addressed to Shinobu Hirai and Haruo Okado, Neural Development Project, Department of Brain Development and Neural Regeneration, Tokyo Metropolitan Institute of Medical Science, Tokyo 156-8506, Japan.

E-mail: hirai-sn@igakuken.or.jp (S.H.) and okado-hr@igakuken.or.jp (H.O.)

Abstract: Psychiatric disorders are considered to be associated with metabolic dysfunction; however, it is unclear whether our current high-sugar diet contributes to pathogenesis. We demonstrate that a high-sucrose diet during adolescence induces psychosis-related phenotypes, such as hyperactivity, poor working memory, impaired sensory gating, and disrupted interneuron function, particularly in mice deficient for glyoxalase-1, an enzyme involved in detoxification of sucrose metabolites. Further, the high-sucrose diet induced microcapillary impairment and reduced brain glucose uptake. Aspirin protected against this angiopathy, enhanced brain glucose uptake, and prevented abnormal behavioral phenotypes. The brains of patients with schizophrenia and bipolar disorder exhibited similar angiopathy. Psychiatric disorders are associated with microvascular brain damage, possibly due to various environmental stresses including metabolic stress.

Introduction:

Considering the global increase in dietary sugar intake, the World Health Organization recently published guidelines that addressed concerns regarding body weight gain and dental caries development (*1*). Body weight gain or high-sugar intake alone increases the risks of numerous chronic diseases, including diabetes, hypertension, and kidney disease. However, studies on the effects of high-sugar intake during adolescence on future mental health are limited. The daily calorie intake from sugar by teenagers is higher than that observed for other age group (~20% of total daily caloric intake) (*2*). Interestingly, most chronic psychiatric disorders, including schizophrenia (SZ) and bipolar disorder (BD) discussed in the present study, develop before the age of 30 years via complex interactions among multiple genetic and environmental risk factors. Therefore, excessive sugar intake may contribute to the pathogenesis of psychiatric disorders during this critical prodromal period. Indeed, sugar consumption of patients with SZ and BD is approximately 2-fold more than age-matched healthy individuals, and patients with SZ who consume more sucrose exhibit worse 2-year outcomes (*3-5*). Moreover, the odds ratios for mental distress, hyperactivity, and behavioral disorders were the highest among adolescents who self-reported the highest consumption of soft drinks compared with the findings in other age groups (*6*).

Advanced glycation end products (AGEs) and reactive carbonyl compounds can be produced from dietary sugars, and these compounds can lead to the production of free radicals and reactive oxygen species (ROS), followed by the induction of oxidative stress and additional AGE formation. There is substantial evidence regarding elevated oxidative stress as measured by ROS accumulation and reduced glutathione levels in patients with psychiatric disorders (*7-9*). Glyoxalase I (GLO1) is an antioxidant zinc metalloenzyme that protects cells from AGE toxicity by catalyzing the binding of the reactive carbonyl compound methylglyoxal to glutathione to form S-lactoyl-glutathione (*10*), which is expressed at lower levels in patients with depressive-state BD and major depressive disorder than in controls (*11*). In addition, a patient exhibiting poor convalescence was found to harbor a frameshift mutation in *GLO1* leading to reduced enzyme activity(*12*, *13*).

Despite the accumulated evidence, it is insufficient to insist that excessive sugar intake contributes to the pathogenesis of psychiatric disorders among susceptible individuals. We addressed this causality by generating mice with psychosis-related phenotypes on the basis of the gene × environment interaction (G × E) approach and assessed whether excessive sucrose consumption during adolescence is a novel environmental risk factor for SZ and BP development. Furthermore, we identified angiopathy as a novel psychiatric disorder phenotype in

both mice with high-sucrose intake and deficient GLO1 activity as well as in brain samples from patients with BD and SZ. Additionally, several phenotypes of psychiatric disease were found to be prevented using anti-inflammatory drug treatment.

Results

Psychosis-related behavioral phenotypes in mice on a high-sucrose diet

To test our hypothesis, we examined mice fed one of two diets containing the same total calories and caloric proportions of carbohydrates, fat, and proteins (Fig. 1A) but with either starch or sucrose as the main carbohydrate. We investigated four groups of mice fed these diets for 50 days immediately after weaning (from postnatal day 21, corresponding to the juvenile/adolescent stage): wild-type (WT) starch-fed mice (control, CTL), WT sucrose-fed mice (environmental stressor, Env), *Glo1* heterozygous knockout starch-fed mice (genetic factor, Gen), and *Glo1* heterozygous knockout sucrose-fed mice (G × E) (Fig. 1A). Reduced GLO1 expression in *Glo1* heterozygous mice was confirmed in the cerebral cortices, including the hippocampus, using western blotting (fig. S1A, B). The body weight trajectories of these mice were similar to those of control mice up to 11 weeks of age, indicative of normal structural development (fig. S1C) and obviating the effects of obesity on the observed group differences described ahead. No significant

differences were observed in open-field locomotor activity (Fig. 1B), pre-pulse inhibition (PPI; a measure of sensory-motor gating) (Fig. 1D), and object location performance (used as a test of working memory) (Fig. 1E) among CTL, Env, and Gen groups. However, G × E mice exhibited greater locomotor activity, impaired PPI, and working memory deficits compared with CTL mice (Fig. 1B, D, E). A decline in acoustic startle responses was observed in *Glo1* heterozygous mice fed either diet compared with WT mice (Fig. 1C). By contrast, self-grooming, nest building, and elevated plus maze activity (a measure of general anxiety) were influenced by diet but not by *Glo1* genotype (Fig. 1F, G, and fig. S2A). No differences in social interaction were detected among groups (fig. S2B).

Higher basal dopamine and greater amphetamine-induced release in the striatum are cardinal characteristics of SZ (*14*, *15*), whereas unbalanced dopamine regulation between the medial prefrontal cortex (mPFC) and striatum has been reported in patients with SZ (*16*). Therefore, we measured dopamine release in the nucleus accumbens (NAc) and mPFC using *in vivo* microdialysis and found both enhanced basal and amphetamine-induced release only in G × E mice in the NAc and decreased basal dopamine release in the mPFC in sucrose-fed mice (Fig. 1H and fig. S2C). Thereafter, to assess whether this enhanced dopamine release induced the observed behavioral phenotypes, we examined the effects of aripiprazole, a D2 receptor partial agonist and

clinical antipsychotic (*17*), administered during the last 7 days (0.5 mg/kg/day) of sucrose feeding (Fig. 1A, I, J and fig. S2D–I). Indeed, the hyper-locomotion and increased striatal dopamine release observed in G × E mice were completely reversed by aripiprazole treatment (Fig. 1I, J). Conversely, the other behavioral defects were not improved by aripiprazole treatment (fig. S2D–I). Therefore, aripiprazole treatment selectively improved abnormalities in G × E mice, which means that these abnormalities were partially caused by dysregulated dopamine signaling.

Dysfunction of parvalbumin-positive inhibitory interneurons in G × E mice

The precisely coordinated activity of parvalbumin (PV)-positive GABAergic interneurons is crucial for the maintenance of PPI and working memory (*18*). We investigated PV expression levels using immunohistochemistry and western blotting for examining whether altered PV interneuron activity contributes to these psychiatric disease-associated phenotypes. The number of PV-positive cells was evidently lower in the hippocampus of sucrose-fed mice than in that of starch-fed mice (Fig. 2A, B) and was the lowest in G × E mice (Fig. 2C, D). Considering that gamma oscillations are produced via the synchronous activation of PV neurons, we measured gamma oscillations (30–45 Hz) using surface electroencephalography (EEG) to examine whether this downregulation of PV was accompanied by functional abnormalities in neural activity.

Sucrose-fed mice exhibited elevated baseline gamma oscillation power compared with starch-fed mice in the home cage (Fig. 2E). Moreover, G × E mice did not exhibit an increase in the gamma oscillation power when approaching a novel object (Fig. 2F). These results are consistent with findings in patients with SZ and BD as well as other mouse models of psychosis demonstrating increased baseline gamma oscillations and decreased sensory stimulus-evoked gamma power (*19*, *20*). In addition, increased gamma oscillation power, required to achieve appropriate cognitive function, is observed in the visual cortex and mPFC of animals and humans during various perceptual and cognitive tasks (*21*, *22*); indeed, such increases were observed in the CTL, Env, and Gen groups (Fig. 2F). Therefore, our results suggest that G × E mice mimic the pathophysiological changes of PV neurons observed in psychiatric disorders.

To summarize, the administration of a high-sucrose diet to *Glo1* heterozygous mice induces behavioral, histological, and pathophysiological phenotypes of psychiatric disorders, suggesting that excessive sucrose intake during adolescence is a potential environmental risk factor.

AGE accumulation and impaired astrocyte function in G × E mice

We assessed neurocellular abnormalities associated with reduced GLO1 expression to investigate the mechanisms underlying the emergence of these psychiatric phenotypes, particularly in G × E

mice. Strong GLO1 expression was detected in astrocytes (fig. S3A–F), especially those surrounding capillaries (fig. S3B, C). By contrast, we observed moderate GLO1 expression in neurons, whereas its expression was below the limit of detection in vascular endothelial cells and microglial cells (fig. S3A–I). Several studies have described GLO1 expression and its effects on the peripheral vasculature; thus, other methods for the detection of GLO1 expression in vascular endothelial cells might be required. GLO1 expression was not detected in the brains of *Glo1* homozygous mice (fig. S3J). Thereafter, immunohistochemical staining was performed, and a stronger fluorescent AGE immunoreactive signal (detected using an ab23722 antibody) was revealed in the vascular endothelial cells of G × E mice compared with CTL mice (Fig. 3A–G). Moreover, we detected another AGE (AGE-4), a product of fructose and carbonyl compounds metabolism, in the microglia of sucrose-fed mice (fig. S4A–E). Compared with the starch-fed groups, microglial AGE-4 accumulation in sucrose-fed groups was accompanied by elevated IBA1 fluorescence intensity and an enlarged CD68-positive area (fig. S4A, F, G, H), both of which are phenotypes identified in activated microglia (*23*, *24*).

Since it was not possible to investigate the accumulation patterns of all AGEs, we focused on astrocytes because these cells exhibit a high GLO1 expression (fig. S3A–F) as well as a well-described reactive phenotype in response to pathogenic conditions including neuroinflammation

characterized by enhanced glial fibrillary acid protein (GFAP) expression. Typically, cellular damage from AGE accumulation is caused by inflammatory responses induced by RAGE activation or by a loss of normal protein function following AGE-forming reactions (*25*). Astrocytic activation was examined in mice expressing green fluorescent protein (GFP) under control of the *GFAP* promoter (*26, 27*). To acquire images, we selected the hippocampal region, which showed extensive GFAP promoter activation in this transgenic mouse; on the other hand, the cortical region showed sparse activation (Fig. 3I). Strongly enhanced *GFAP* promoter function was observed in G × E mice, without changes in the number of GFAP-positive astrocytes (Fig. 3H–K), indicating that the astrocytes in G × E mice are in the reactive pre-condition during the high-sucrose feeding (*28, 29*). Taken together, AGE accumulation occurred in cells with weak GLO1 expression (Fig 3A–G and fig. S3, 4) and astrocytes exhibited pre-inflammatory status in GLO1-deficient mice fed a high-sucrose diet (Fig 3H–K).

Microcapillary angiopathy and impaired glucose intake in G × E mice

Endothelial AGE accumulation and astrocyte reactivity may impair the blood–brain barrier (BBB) function, because they contribute the BBB function that tightly controls the parenchymal environment by modulating the selective passage of nutrients and various factors (*30*). To

examine changes in the endothelial function, we first conducted a transcriptome analysis of the prefrontal cortex (PFC), a region strongly implicated in psychiatric impairments, using microarrays (Fig. 4A, B). The coagulation factor V, essential for the production of fibrin from fibrinogen, ranked seventh on the list of transcripts exhibiting more than doubled expression in G × E mice compared with the other three groups (Fig. 4A, Supplementary Table 1, 2). Fibrin controls hemostasis via polymerization with platelets to form blood clots and deposits of this protein are indicative of endothelial abnormality regardless of the nature of the inciting event (i.e., mechanical insult, infection, or immunological derangements) (*31*). In the early stage of endothelial cell impairment, fibrin accumulates in the capillaries. Therefore, we investigated vascular fibrin accumulation using immunohistochemistry and confirmed the presence of significant fibrin accumulation on the vascular lumen side of endothelial cells in the brain capillaries of G × E mice (Fig. 4C–F). Fibrin deposition in the brain parenchyma, as observed in Alzheimer's disease, was not detected in G × E mice, indicating that physical BBB disruption did not occur (*32*).

Thereafter, we speculated that the abnormal vascular endothelial cells observed in G × E mice could alter glucose uptake from the plasma into the brain parenchyma. Extracellular glucose concentrations in the brain parenchyma were measured under three conditions: 1) fasting, 2) 1 h

after eating, and 3) 2 h after eating. Glucose concentrations in the parenchyma was significantly lower in G × E mice compared with the other groups at 1 h after eating (Fig. 4G). We measured the vascular diameter and glucose transporter 1 expression, the major glucose transporter expressed in vascular endothelial cells, and observed no difference among the four groups (fig. S5). Further, no differences were noted in plasma glucose and fasting plasma insulin levels among the four groups (Fig. 4H, I), indicating that this lower parenchymal glucose concentrations in G × E mice is due to reduced uptake across the BBB rather than dysregulation of plasma glucose or insulin signaling.

Protective effects of chronic low-dose aspirin against behavioral abnormalities and angiopathy

Previous reports have shown that adjunct non-steroidal anti-inflammatory drug (NSAID) treatment can improve psychiatric disorder scores (*33*, *34*). Aspirin, an NSAID, is routinely used for the prevention and alleviation of vascular-related adverse events associated with high blood pressure, ischemia, and cardiovascular diseases (*35*, *36*). Therefore, we examined whether aspirin treatment can protect against the development of abnormal behaviors in G × E mice (Fig. 1A, Fig. 5A–D and fig. S6A–C). Low-dose aspirin (1 mg/kg/day) prevented hyperlocomotor activity

and deficits in PPI, working memory, and grooming duration among G × E mice (Fig. 5A–D) but did not improve nest building and elevated plus maze scores (fig. S6B, C). These behavioral improvements were accompanied by a decrease in endothelial fibrin accumulation (Fig. 5E, F) and a partial restoration of glucose intake into the brain parenchyma (Fig. 5G). Collectively, these results suggest that aspirin treatment in G × E mice provides healthy brain function that is accompanied by improvement of angioplasty and brain glucose availability.

Angiopathy in postmortem brains of patients with psychiatric disorders

Finally, we compared immunostaining of brain slices from healthy controls and patients with SZ or BD to examine whether these patients exhibit this angiopathic fibrin accumulation in vascular endothelial cells. Consistent with the findings in G × E mice, these patients exhibited significantly elevated fibrin accumulation in the vascular endothelium (Fig. 6A–C). Therefore, this fibrin-related angiopathy may contribute to disease progression, despite the absence of *GLO1* gene mutation and lack of specific evidence for higher sugar intake compared with controls, suggesting vascular damage as a novel and common phenotype of psychiatric illness.

Discussion

We demonstrated that high dietary sucrose consumption during adolescence is a potential risk factor for the development of neurofunctional and behavioral phenotypes related to psychiatric illnesses, such as SZ and BD, including impaired sensory gating, interneuron dysfunction and working memory, hyperactivity, and greater basal and stimulus-evoked striatal dopamine release. Second, we identified endothelial fibrin accumulation ("angiopathy") in both model mice expressing these psychosis-related phenotypes and in the postmortem brains of patients with SZ or BD. Third, we observed that glucose intake from the plasma into the brain parenchyma was impaired in G × E mice, potentially because of angiopathy. Finally, we found that chronic low-dose aspirin treatment prevented fibrin deposition in the capillaries, improved glucose transport, and reversed several of the behavioral phenotypes in G × E mice, suggesting sucrose-induced angiopathy as a seminal pathogenic event in mental illness.

A possible pathogenic mechanism for dietary sucrose-induced toxicity among *GLO1* heterozygous mice is illustrated in Fig. 6D. Sucrose consists of glucose and fructose, and AGEs and pre-AGE carbonyl compounds, such as glyceraldehyde and methylglyoxal, are more readily generated from fructose than from glucose (*37*). Moreover, in cerebrospinal fluid, fructose concentration may be controlled by mechanisms distinct from that in plasma as its levels are higher, whereas glucose levels are lower in this compartment compared with those in plasma

(*38*). Fructose-derived pre-AGE carbonyl compounds were presumably rapidly detoxified by GLO1 in astrocytes because these cells maintain strong GLO1 expression (fig. S3A–F). Alternatively, endothelial cells and microglia exhibit weak GLO1 expression in WT mice (fig. S3D–I), which may result in excessive carbonyl compound and AGE accumulation, leading to a pro-inflammatory response in astrocytes via RAGE signaling or cytokine release from microglia. Consequently, this perivascular inflammation can lead to angiopathy and poor glucose uptake, resulting in damage to various neuronal populations, particularly in PV-containing interneurons (*39*) (Fig. 2, Fig. 4). Indeed, abnormal glucose transport was associated with endothelial cell pathology and astrocyte reactivity predominantly in *Glo1* heterozygous mice fed a high-sucrose diet (Fig. 3, Fig. 4). Furthermore, the NSAID aspirin protected against the emergence of angiopathy as evidenced by the reduced fibrin accumulation and partially restored parenchymal glucose concentration as well as prevented several behavioral phenotypes of psychiatric illness, possibly by reducing inflammation and oxidative stress (Fig. 5 and fig. S6).

The PV neuron dysfunction in G × E mice may be caused by the unique properties of these cells. Parvalbumin-expressing interneurons exhibit a lower input resistance and higher-amplitude rapid after-hyperpolarization than several projection neurons, and this combination of properties generates higher frequency action potentials compared with those by other neuron types. To

maintain this rapid spiking, PV neurons require high energy expenditure as evidenced by mitochondrial and cytochrome c oxidase enrichment (*40*). Therefore, reduced glucose within the brain parenchyma may preferentially disturb PV neuron function. Furthermore, robust PV neuron function is required for PPI, working memory, amphetamine-induced hyper-locomotion, dopamine (or 3,4-dihydroxyphenylacetic acid) regulation, and gamma oscillation generation, all of which are considered core symptoms of psychiatric disorders. Indeed, reduced PV neuron number has been reported in postmortem brains of patients with psychiatric disorders such as SZ and BP (*41-43*). Further, the inhibitory activity of PV neurons is critical under environmental stress to prevent a sequela of excessive excitatory activity such as oxidative stress and inflammation (*39*). Pathogenic processes might more readily occur during the critical adolescent prodromal period, wherein PV neurons may have increased vulnerability because of delayed maturation, which is another feature of PV neurons (*44*).

In the present study, we identified capillary angiopathy in both G × E mice and the postmortem brains of patients with SZ and BD (Fig. 4C–F, Fig. 6A–C). Although the angiopathy observed in G × E mice was probably caused by the combined high AGE production capacity of fructose and GLO1 deficiency, neither of these conditions were necessarily present in the patient sample. However, various environmental stresses may converge to induce angiopathy. Several

studies have reported that stressors, such as social defeat, isolation, and viral infection, induce vascular defects (*45*-*47*). It should be noted that these same stressors are risk factors for SZ and BD as well and induce PV neuron hypofunction, a core phenotype of these diseases (*48*), suggesting that angiopathy is a common trigger for psychiatric phenotypes. Further extensive research is warranted to prove this hypothesis.

Chronic treatment with low-dose aspirin mitigated angiopathy (fibrin deposition) and impaired glucose transport into the brain parenchyma as well as prevented the emergence of most psychiatric disease-associated behavioral phenotypes, including working memory impairment (Fig. 5). These effects may be attributed to irreversible inhibition of platelet cyclooxygenase-1 and cyclooxygenase-2 activities and thromboxane production, leading to reduced clot formation, as well as the suppression of oxidative stress via the inhibition of NADPH oxidase (NOX)-mediated ROS production by endothelial cells and downstream inhibition of the TNF-α thrombin and the AGE-activated transcriptional factor NF-κB (*49*). Aspirin exerts antioxidative effects on vascular cells (*50*), and it may prevent positive feedback between AGE and ROS production in G × E mice (*51, 52*). Because oxidative stress is a common characteristic of psychiatric disorders (*7, 8, 53*), aspirin may provide protection against disease pathogenesis.

The high-sucrose diet induced several abnormal phenotypes even in WT mice, including impaired nest building skill, excessively prolonged grooming, reduced PV neuron numbers, and elevated gamma oscillation power in the home cage (Fig. 1F–G, 2A–E), indicating that a high-sucrose diet during adolescence may adversely influence high brain function even in the absence of genetic factors predisposing to serious mental illness. On the other hand, the experiments of combination of high-sucrose feeding and other risk genes or environmental stresses will clarify the importance of diet control during adolescence.

Acknowledgments: We thank Sayaka Ogikubo, Yoshie Matsumoto, Haimei Zhang, Minami Murata, Izumi Nohara, Yukiko Shimada, Emiko Hama, Nanako Obata, Mai Hatakenaka, and Chikako Ishida for their contribution to experiments related to this research. We also thank Dr. Tohru Kodama for explaining the procedures for microdialysis and encephalogram recording. We are grateful to Drs. Jun Horiuchi and Kenji Tanaka for reviewing the study. We acknowledge Chiaki Watanabe and Hiromi Onuma for coordinating the donations of postmortem brains. Further, we thank Prof. Hideki Chiba for the preparation of postmortem brain samples. We express our gratitude to the families of the deceased individuals for the donations of brain tissue and their time and effort devoted to the consent process and interviews.

Funding: This work was supported by the Japan Society for the Promotion of Science (KAKENHI grants 18K14832 to S.H., 17K18395 and 19K08033 to H.M., 17K16408 to T.T., and 18H02537 and 18K19383 to H.O.); the Ichiro Kanehara Foundation, Japan Prize Foundation, and Takeda Science Foundation (to S.H.); the Strategic Research Program for Brain Sciences from AMED (grant JP19dm0107107 to H.Y.); and a Grant-in-Aid for Scientific Research on Innovative Areas from the MEXT (JP16H06277 to H.Y.). This research was also supported by KAKENHI Grant Numbers 16H05380 (to M.A.), 18K06977 (to K.T.), 19H03589 (to M.I.), and 18K15354 (to K.S.) as well as AMED Grant Number JP19dm0107088 (to M.I.). This study was also supported by The Kanae Foundation for the Promotion of Medical Science (to K.T.) and The Uehara Memorial Foundation (to M.A.).

Author contributions: S.H. and H.O. designed the study. S.H. performed and analyzed all experiments. H.M. assisted with the experimental design of EEG recording and analysis of the results and edited the manuscript. T.T. coordinated the EEG recording. Y.K., M.H., R.I., A.N., and H.Y. helped with the design of experiments using human specimens and provided fixed human brain sections. T.S. performed data and image analysis. T.N. and S.S. provided GFAP-

GFP mice. T.D. and T.M. generated and provided *Glo1* knockout (KO) mice. K.T. and K.S. backcrossed *Glo1* KO mice to B6J mice for all experiments. Y.N. performed cDNA microarray analysis of gene expression. H.S. assisted with behavioral experiments. M.I., M.A., K.T., K.S., and M.M. provided important suggestions to this study. S.H. generated all figures, tables, and wrote the manuscript. H.O. edited the manuscript and supervised this study.

Competing interests: The authors declare no competing interests.

Data and materials availability: All materials used in this paper are available upon request. The accession number for transcriptome analysis data is provided in the Materials and Methods.

Materials and Methods

Animals

All experimental procedures were approved by the Animal Experimentation Ethics Committee of the Tokyo Metropolitan Institute of Medical Science (49040). All mice were maintained under a 12:12 h light:dark cycle (lights on at 8:00 AM) with free access to the indicated diet. All efforts were made to minimize the number of animals used and their suffering. *Glo1* knockout mice were generated as described previously (*54*). Briefly, *Glo1*-trapped ES cell lines from the International Gene Trap Consortium were used for the generation of 3 founder mice, which were then backcrossed to C57BL/6 mice. Alternatively, mice were backcrossed to GFAP-GFP mice to monitor astrocyte activation. Male mice were exclusively used in the behavioral tests, whereas mice of both sexes were used in histological, biochemical, and physiological experiments.

Diet preparation

The two diets used in the present study were newly created in collaboration with Oriental Yeast Co. Ltd. (Tokyo, Japan). We named the sucrose diet HSD-70 (# OYC 2405100) and the starch diet HCD-70 (# OYC 2405000) (Supplementary Table 4). They contained the same caloric

proportions of carbohydrate, fat, and protein; however, all carbohydrate calories are derived from either starch or sucrose.

Drug preparation

Aripiprazole was dissolved in acetic acid and diluted to 3.5 mg/L in water for administration at 0.5 mg/kg/day. The final acetic acid concentration in the drinking water was 0.7%. Aspirin was dissolved in ethanol and diluted to 70 mg/L in water for administration at 1 mg/kg/day. The final ethanol concentration in the drinking water was 0.15%. The daily dose was based on the measurement of mean water consumption daily in all sucrose-fed *glo1* heterozygous mice and starch-fed wild-type (WT) mice (fig. S1D, E). There were no between-group differences in terms of aripiprazole consumption (Student's *t*-test, Starch +/+ and Suc *glo1*/+: $p = 0.86$) or aspirin-containing water (Student's *t*-test, Starch +/+ and Suc *glo1*/+: $p = 0.61$).

Behavioral tests

Mice were habituated in the behavioral room for >30 min before each test. Behavioral tests were performed in the following sequence of increasing stress: elevated plus maze, grooming, nest building, open field, object location, social interaction, and pre-pulse inhibition (PPI). All test

apparatuses were cleaned using 70% ethanol and water between trials, and the subsequent test session was started only after the ethanol vapor odors had disappeared and the apparatuses had dried.

The elevated plus maze (EPM-04M, Muromachi, Japan) consisted of two opposing open arms (297 × 54 mm) and two closed arms (300 × 60 × 150 mm) extending from a central platform (60 × 60 mm). The entire apparatus was elevated 400 mm above the floor. Each mouse was placed on the central platform facing a closed arm and allowed to freely explore the maze for 10 min. Arm entry was defined as the entry of all four paws into the arm. The time spent in the open arms over 10 min was recorded as an index of state anxiety.

For the self-grooming test, all mice housed in the same home cage were moved into a new cage for 10 min. Each mouse was then individually placed in a standard mouse home cage (31 × 16.5 × 14 cm) illuminated at ~200 lux. After a 10-min habituation period, each mouse was scored for cumulative time spent grooming all body regions (*55*) over 10 min using a stopwatch. Self-grooming behavior is conserved across species and is indicative of certain pathological conditions or factors. In humans, for example, self-grooming increases during stressful conditions and in certain psychiatric disorders (*55*).

For the nest building test, 200 g of corncob was spread across the bottom of each cage for bedding, and a square-shaped piece of cotton was placed in the cage center as raw material for the nest. Each mouse was individually placed in the cage for 8 h. Photos of the constructed nest were acquired every 2 h, and the nest building process was evaluated by measuring the proportion of loose cotton as follows: 1 point for 25% weight (Wt%) loosened, 2 points for 50 Wt% loosened, 3 points for 75 Wt% loosened, and 4 points for 100 Wt% loosened. After 8 h, we checked the shape of the nest and added 1 point if the mice had completed a nest with a bird's nest-like shape. The temperature of the room was maintained at 25°C and illumination at 150–180 lux during nest building. Nest-building behavior is an indicator of general well-being in mice (*56*), whereas poor nest building is an indicator of psychological or physiological abnormalities (*57*, *58*).

For the open field (OF) test, each mouse was placed in the center of the apparatus (40 × 40 × 40 cm; 150–180 lux illumination) and allowed to move freely for 10 min. The behavior of each mouse was monitored using a charge-coupled device camera mounted on the ceiling above the OF. The total distance traveled (cm) was measured using CompACT VAS software (Muromachi).

For the object location test (OLT) of working memory (*59*), mice first explored the empty OF box, and then, two identical objects A and B (two 500-mL PET bottles filled with blue-

colored water) were placed in two corners 5 cm from the wall. After a 10-min exploration/learning period, the mice were returned to their home cage for 5 min, and Object A was moved to a new corner (Object A′). The animals were then placed back in the OF box and allowed to explore for 5 min. The time spent exploring A′ and B were measured to calculate a discrimination index representing working memory according to the following equation: Discrimination Index = (Novel Object A′ exploration time − Familiar Object B exploration time) / (Novel Object A′ + Familiar Object B exploration times). The OLT was performed under illumination at 10–15 lux.

The social interaction test was conducted as previously described (*60*) using a specialized Sociability Apparatus (SC-03M, Muromachi). The time spent sniffing a novel stimulus mouse or object was manually scored from videos recorded using an overhead color USB camera (aa000080a02, Iroiro House). Stimulus mice (129Sv/SvJcl strain) age- and sex-matched to test mice were habituated to the apparatus and to the enclosure cup for 30 min per day for 2 days prior to testing. The location (left or right) of the novel object and novel mouse within an enclosure were alternated across test subjects. The test mouse was allowed to acclimate to the apparatus for a total of 20 min before the sociability test—the first 10 min in the central chamber with the doors closed and then 10 min in the empty arena with the doors open. The test subject

was briefly confined to the center chamber while a novel stimulus mouse in an enclosure cup was placed on one of the side chamber and another empty enclosure cup (novel object) was placed on the other side of the chamber. The test subject was allowed to approach the novel object or mouse freely for 10 min. The time spent interacting with the stimulus mouse versus the novel object was calculated as an index of sociability.

The SR-LAB-Startle Response System (San Diego Instruments) was used to detect acoustic startle reflexes and PPI. Startle responses were measured using 5 stimulus intensities (80, 90, 100, 110, and 120 dB) delivered 10 times each for 40 ms over a white noise background (65 dB). The stimuli were presented in quasi-random order at random inter-trial intervals (10–20 s). In the PPI session, mice were exposed to 2 stimulus patterns: 1) a startle stimulus alone (120 dB, 40 ms) with no pre-pulse stimulus and 2) a startle stimulus (120 dB, 40 ms) following a pre-pulse stimulus (70 dB for 20 ms; lead time, 100 ms). Each trial was repeated 10 times in quasi-random order at random inter-trial intervals (10–20 s). PPI was defined as the percent decline in startle response because of pre-pulse stimuli according to the following equation: 100 − [(120 dB startle amplitude after any pre-pulse) / (120 dB startle amplitude only)] × 100.

Immunohistochemistry

Following transcardial perfusion with PBS and 4% paraformaldehyde, entire brains were collected, post-fixed at 4°C overnight, and cryoprotected in 20% sucrose at 4°C overnight. Serial coronal sections (50 μm) were then cut using a cryostat (CM3050 S; Leica Microsystems). The antigens in the tissues were reactivated by heating in HistoVT One solution (Nakalai Tesque) for 30 min at 70°C using a water bath. Sections were permeabilized with 0.2% Triton X-100 and 1% Block Ace (DS Pharma Biomedical) in PBS for 30 min at room temperature, following which they were incubated overnight with the indicated primary antibodies at room temperature. For immunohistochemistry of postmortem human brain tissues, paraffin blocks including BA9 (a region of frontal cortex) were sliced into 10-μm sections, deparaffinized with xylene, and rehydrated with decreasing concentrations of ethanol in water. Antigens were reactivated by heating in HistoVT One solution for 30 min at 90°C using a water bath. Sections were treated with TrueBlack Lipofuscin Autofluorescence Quencher (Biotium Inc.) for 30 s at room temperature and blocked with 1% Block Ace (DS Pharma Biomedical) in PBS for 30 min at room temperature. Thereafter, the mouse and human brain sections were subjected to the same immunostaining procedures. The following primary antibodies were diluted in PBS containing 0.4% Block Ace: goat anti-PV (Frontier Institute, PV-Go-Af860; 1:2000), mouse anti-ALDH1L1 (Rockland, 600-101-HB6S; 1:200), FITC-conjugated tomato lectin (VECTOR, FL-1171; 1:200),

chick anti-GFP (Abcam, ab13970; 1:500), goat anti-IBA1 (Abcam, ab48004; 1:100), mouse anti-NeuN (Millipore, MAB377; 1:500), rabbit anti-AGE (Abcam, ab23722; 1:2000), rabbit anti-IBA1 (Wako, WDJ3047; 1:300), rat anti-CD68 (Abcam, ab53444; 1:500), and rabbit anti-fibrin (Dako, A0080, 1:500). Thereafter, sections were washed three times with PBS–0.05% Tween-20, incubated for 2 h with fluorochrome-conjugated secondary antibodies in PBS containing 0.4% Block Ace, and washed an additional three times in PBS containing 0.4% Block Ace. For enhanced horseradish peroxidase (HRP) immunostaining, samples were treated with 3% H_2O_2 in PBS for 20 min following the reactivation step to quench endogenous peroxidase activity and washed in PBS. Sections were incubated with rabbit anti-GLO1 (Novusbio, NBP2-75514, 1:1500) and/or mouse anti-AGE4 (Trans Genic Inc, 14B5, 1:400), followed by incubation with anti-IgG antibodies conjugated to biotin (Vector, 1:200). After washing as described for other secondary antibodies, sections were incubated with streptavidin-conjugated HRP (Jackson ImmunoResearch, 1:200) for 120 min and washed three times with PBS–0.05% Tween-20. The TSA Plus Fluorescence System (PerkinElmer) was used to detect HRP activity. All preparations were counterstained with DAPI (Nacalai Tesque) to reveal cell nuclei, washed three additional times, mounted in Permaflow (Thermo Scientific), and observed using a FluoView® FV3000

Confocal Laser Scanning Microscope (Olympus). A Keyence BZ-X800 microscope was used for tilling image acquisition as presented in Fig. 3I.

Image analysis

Unless otherwise noted, all image analyses were performed using ImageJ version 2.0.0-rc-59/1.51n, and images were first binarized. PV-positive cells with a threshold exceeding 30 were counted.

To measure the areas immunopositive for AGE, fibrin, and AGE4, the threshold settings were applied to ensure that only the correct immunopositive area was properly selected, and the stained area of the entire screen was measured. For measuring the fluorescence intensity of GFP and IBA1, after setting the ROI to select only target immunoreactive cells, the intensity of >5 cells in each image was measured. To count microglial cells containing a CD68-positive area exceeding 20 μm^2, the threshold was set to select only the CD68-positive area. Colocalization analysis of two different fluorescence markers was performed using the Fiji plug-in Coloc 2 with the default settings. We adopted Pearson's R below the threshold to judge colocalization.

Immunoblotting

Extracts from mouse hippocampi were homogenized in lysis buffer containing 40 mM Tris base, 0.4% sodium dodecyl sulfate (SDS), 0.01 M EDTA (pH 8.0), 8 M urea, and 1 mM phenylmethylsulfonyl fluoride. The total lysate protein content was quantified using a DC Protein Assay Kit (Bio-Rad). Total protein (30 µg per gel lane) was separated using SDS–PAGE and transferred to PVDF membranes (Millipore). Membranes were blocked with TBST buffer (1.37 M NaCl, 2.7 mM KCl, and 0.25 M Tris, pH 8.0) including 0.2% Triton X-100 and 5% bovine serum albumin (BSA) for 30 min at room temperature with slow shaking, followed by incubation overnight with primary antibodies in TBST including 2% BSA at 4°C. The primary antibodies used were rabbit anti-GLO1 (Santa Cruz, sc-67351; 1:1000), mouse-anti-PV (Swant, PV-235; 1:1000), rabbit anti-glucose transporter 1 (Glut1, Frontier Institute, Af1020; 1:1000) and mouse anti-tubulin (Santa Cruz, sc-32293; 1:10000). After washing three times with TBST, membranes were incubated with the secondary antibody (HRP-conjugated anti-mouse or anti-rabbit IgG antibody, GE Healthcare; 1:2000) in TBST plus 2% BSA. After washing three times with TBST, blots were processed for chemiluminescence using standard protocols (ECL Prime Western Blotting Detection Regent #RPN2236, GE Healthcare), and signals were detected using a LAS 4000 Imager (Fuji Film).

Microdialysis

We used an in vivo microdialysis system for the measurement of extracellular dopamine concentration (*61*) and collection of brain parenchymal dialysate. After anesthesia by intraperitoneal injection of ketamine (80 mg/kg)/xylazine (16 mg/kg), mice were fixed in a stereotaxic apparatus (Narishige) and a microdialysis guide cannula (CXG-8, Eicom) was implanted in the medial prefrontal cortex (mPFC; antero-posterior (AP), +1.8 mm; medio-lateral (ML), ±0.15 mm; dorso-ventral (DV), −1.5 mm from bregma), or nucleus accumbens (NAc) (AP, +1.5 mm; ML, ±0.6 mm; DV, −3.5 mm from bregma). After recovery for at least 10 days, a microdialysis probe (CX-I-8-01 for the mPFC and CX-I-8-02 for NAc; Eicom) was inserted via the guide cannula. Following insertion, the probe was connected to a syringe pump and perfusion was performed at 2 μL/min for NAc and 0.5 μL/min for mPFC using Ringer's solution (147 mM NaCl, 4 mM KCl, and 2.3 mM $CaCl_2$). Dialysate samples were collected every 10 min and automatically loaded onto an HTEC-500EPS HPLC unit (Eicom). Constant 5-HT concentration in three consecutive collection periods was first confirmed to rule out blood contamination before initiating the measurements of dopamine concentration or collection of parenchymal dialysates. Analytes were then separated on an affinity column (PP-ODS III, Eicom), and compounds were subjected to redox reactions within an electrochemical detection unit (amperometric DC mode;

applied potential range, 450 mV). The resulting chromatograms were analyzed using an EPC-500 data processor (Eicom), and actual sample concentrations were computed based on the peak heights obtained using 0.01, 0.1, and 1 pg dopamine in standard solution (Sigma). The locations of the microdialysis probes were histologically confirmed.

EEG recordings

For behavioral and video/EEG monitoring, mice were anesthetized by an intraperitoneal injection of ketamine (80 mg/kg)/xylazine (16 mg/kg), fixed in a stereotaxic apparatus (Narishige, Japan), and implanted with EEG and electromyography (EMG) electrodes. The EEG electrodes were gold-coated stainless steel screws (SUS303) soldered with lead wires (ANE-0190, Adler's Nest, Japan) implanted epidurally over the left frontal cortex (AP, 1 mm; ML, 1 mm) and the bilateral parietal cortex (AP, −2 mm; ML, ±2 mm). All wires were soldered to a multichannel electrical connector (R833-83-006-001, TOKIWA SHOKO, Japan). The left parietal cortex electrode was used as a reference for monitoring the frontal cortex EEG. The EMG electrodes were lead wires placed bilaterally into the trapezius muscle. Following recovery for at least 10 days, EEG/EMG signals were amplified and band-pass filtered (EEG: 1.5–1000 Hz; EGM: 15–3000 Hz) using a MEG-6116 system (NIHON KOHDEN), digitized at a sampling rate of 200 Hz, recorded using a

data acquisition system (PowerLab 8/30, ADInstruments), and analyzed using LabChart Software (ADInstruments). Behavioral activities were recorded using a USB camera (aa000080a02, Iroiro House, Japan). Behavioral and electrophysiological responses to a novel object (an empty 100 mL DURAN bin) were recorded in an OF chamber (20 × 20 × 26 cm). The novel object was placed in one corner of the OF chamber to induce exploration. The 30 s preceding the first contact with the novel object was analyzed for object recognition ("object activity"). For EEG monitoring in the home cage, mice were first habituated for 8 h. Home cage EEG data were then acquired for 2 min after awaking as confirmed by clear EMG signals and movement images from an offline video camera analysis ("home cage activity"). All recordings were converted into power spectra using a fast Fourier transform (FFT) algorithm with a 5-s Hann cosine-bell window and 50% overlap between successive window measurements. All FFTs were maintained at 1024 points to obtain 0.512 Hz resolution. The total signal amplitude or power (V^2) in each 5-s period was measured as the power magnitude at each frequency. The mean of the grouped power spectra was calculated over the following frequency ranges: 1–4 Hz (delta), 5–10 Hz (theta), 30–45 Hz (low gamma), and 55–80 Hz (high gamma). The power values detected at each frequency range for 30 s were further averaged over 30 s of total EEG power using the mean values to

remove potential noise. These analyses were performed using custom software written in MATLAB (R2019b; MathWorks).

Transcriptome analysis

Three independent total RNA samples from each group were mixed and purified using a RNeasy Mini Kit (Qiagen). RNA quality was assessed using a 2100 bioanalyzer (Agilent Technologies). Cy3-labeled cRNA was prepared using a Low Input Quick Amp Labeling Kit (Agilent Technologies), in accordance with the manufacturer's protocol. Samples were hybridized to the SurePrint G3 Mouse Gene Expression v2 Microarray (G4852B; Agilent Technologies). Thereafter, the array was washed and scanned using the SureScan Microarray Scanner (Agilent Technologies). Microarray images were analyzed using the Feature Extraction software with default settings for all parameters (Agilent Technologies). Data from each microarray analysis were normalized by shift to the 75th percentile without baseline transformation. Microarray results were deposited in the Gene Expression Omnibus database under the accession number GSE141829.

Insulin and glucose measurements

Blood plasma was collected from the mouse cheek as described by Golde (*62*). Plasma glucose concentration was measured using a Precision-Neo blood glucose meter (#71386-80, Abbott Japan), plasma insulin concentration using an ELISA kit (#M1102, MORINAGA), and glucose concentration in the dialysate samples using a different ELISA kit (#ab65333, Abcam), all according to the manufacturers' instructions. Data were collected on a microplate reader (Varioskan, Thermo Fisher Scientific).

Human postmortem brain tissue collection

Postmortem brain tissues from patients with SZ and BD were obtained from the Fukushima Brain Bank at the Department of Neuropsychiatry, Fukushima Medical University. Postmortem brain tissues from control individuals were obtained from the Section of Pathology, Fukushima Medical University Hospital. The use of postmortem human brain tissues in the present study was approved by the Ethics Committee of Fukushima Medical University (No.1685) and Tokyo Metropolitan Institute of Medical Science (No. 18-20) and complied with the Declaration of Helsinki and its later amendments. All procedures were conducted with the informed written consent of the next of kin. Detailed demographic information of the 10 patients with SZ, 9 patients with BD, and the 12 age- and sex-matched control individuals is provided in Supplementary Table

3. No between-group differences were observed in terms of sex (Fisher's exact test, Ctrl and SZ: $p = 1.00$, Ctrl and BD: $p = 0.40$), age (Student's t-test, Ctrl and SZ: $p = 0.69$, Welch's t-test, Ctrl and BD: $p = 0.66$), postmortem interval (Student's t-test, Ctrl and SZ: $p = 0.89$, Ctrl and BD: $p = 0.98$), or a history of diabetes mellitus (Fisher's exact test, Ctrl and SZ: $p = 0.59$, Ctrl and BD: $p = 0.59$). Each patient with SZ and BD fulfilled the diagnostic criteria established by the American Psychiatric Association (Diagnostic and Statistical Manual of Mental Disorders, DSM-IV) and did not have a past history of other neurological disorders or substance abuse. Moreover, none of the control individuals had any record of mental disorders, neurological disorders, or substance abuse.

Statistical analyses

Student's *t*-test was used to analyze the results presented in fig. S1D and E. Statistical differences among ≥4 groups were determined using one-way analysis of variance (ANOVA), two-way ANOVA, three-way ANOVA, or repeated-measures ANOVA, followed by the Bonferroni multiple comparison test or Tukey–Kramer test as a post-hoc test, as summarized in Supplementary Table 5. Behavioral results from the Starch +/+ and Suc *glo*1/+ groups were reused according to the 3R rule. The number of animals used can be found in the legend of each figure. All data are presented as the mean ± SEM. A p-value of <0.05 denoted statistical

significance.

References

1. *Sugar Intake for adults and children* (2015).
2. N. Fidler Mis, C. Braegger, J. Bronsky, C. Campoy, M. Domellöf, N. D. Embleton, I. Hojsak, J. Hulst, F. Indrio, A. Lapillonne, W. Mihatsch, C. Molgaard, R. Vora, M. Fewtrell, Sugar in Infants, Children and Adolescents: A Position Paper of the European Society for Paediatric Gastroenterology, Hepatology and Nutrition Committee on Nutrition. *J Pediatr Gastroenterol Nutr* **65**, 681-696 (2017).
3. M. Peet, International variations in the outcome of schizophrenia and the prevalence of depression in relation to national dietary practices: an ecological analysis. *Br J Psychiatry* **184**, 404-408 (2004).
4. J. C. Ratliff, L. B. Palmese, E. L. Reutenauer, E. Liskov, C. M. Grilo, C. Tek, The effect of dietary and physical activity pattern on metabolic profile in individuals with schizophrenia: a cross-sectional study. *Compr Psychiatry* **53**, 1028-1033 (2012).
5. J. L. Elmslie, J. I. Mann, J. T. Silverstone, S. M. Williams, S. E. Romans, Determinants of overweight and obesity in patients with bipolar disorder. *J Clin Psychiatry* **62**, 486-491; quiz 492-483 (2001).
6. L. Lien, N. Lien, S. Heyerdahl, M. Thoresen, E. Bjertness, Consumption of soft drinks and hyperactivity, mental distress, and conduct problems among adolescents in Oslo, Norway. *Am J Public Health* **96**, 1815-1820 (2006).
7. A. Ciobica, M. Padurariu, I. Dobrin, C. Stefanescu, R. Dobrin, Oxidative stress in schizophrenia - focusing on the main markers. *Psychiatr Danub* **23**, 237-245 (2011).
8. B. K. Bitanihirwe, T. U. Woo, Oxidative stress in schizophrenia: an integrated approach. *Neurosci Biobehav Rev* **35**, 878-893 (2011).
9. L. G. Nucifora, T. Tanaka, L. N. Hayes, M. Kim, B. J. Lee, T. Matsuda, F. C. Nucifora, Jr., T. Sedlak, R. Mojtabai, W. Eaton, A. Sawa, Reduction of plasma

glutathione in psychosis associated with schizophrenia and bipolar disorder in translational psychiatry. *Transl Psychiatry* **7**, e1215 (2017).

10. P. J. Thornalley, Glutathione-dependent detoxification of alpha-oxoaldehydes by the glyoxalase system: involvement in disease mechanisms and antiproliferative activity of glyoxalase I inhibitors. *Chem Biol Interact* **111-112**, 137-151 (1998).
11. M. Fujimoto, S. Uchida, T. Watanuki, Y. Wakabayashi, K. Otsuki, T. Matsubara, M. Suetsugi, H. Funato, Y. Watanabe, Reduced expression of glyoxalase-1 mRNA in mood disorder patients. *Neurosci Lett* **438**, 196-199 (2008).
12. M. Miyashita, M. Arai, A. Kobori, T. Ichikawa, K. Toriumi, K. Niizato, K. Oshima, Y. Okazaki, T. Yoshikawa, N. Amano, T. Miyata, M. Itokawa, Clinical features of schizophrenia with enhanced carbonyl stress. *Schizophr Bull* **40**, 1040-1046 (2014).
13. M. Toyosima, M. Maekawa, T. Toyota, Y. Iwayama, M. Arai, T. Ichikawa, M. Miyashita, T. Arinami, M. Itokawa, T. Yoshikawa, Schizophrenia with the 22q11.2 deletion and additional genetic defects: case history. *Br J Psychiatry* **199**, 245-246 (2011).
14. O. D. Howes, A. J. Montgomery, M. C. Asselin, R. M. Murray, P. M. Grasby, P. K. McGuire, Molecular imaging studies of the striatal dopaminergic system in psychosis and predictions for the prodromal phase of psychosis. *Br J Psychiatry Suppl* **51**, s13-18 (2007).
15. M. Laruelle, A. Abi-Dargham, C. H. van Dyck, R. Gil, C. D. D'Souza, J. Erdos, E. McCance, W. Rosenblatt, C. Fingado, S. S. Zoghbi, R. M. Baldwin, J. P. Seibyl, J. H. Krystal, D. S. Charney, R. B. Innis, Single photon emission computerized tomography imaging of amphetamine-induced dopamine release in drug-free schizophrenic subjects. *Proc Natl Acad Sci U S A* **93**, 9235-9240 (1996).
16. G. Winterer, D. R. Weinberger, Genes, dopamine and cortical signal-to-noise ratio in schizophrenia. *Trends Neurosci* **27**, 683-690 (2004).
17. A. de Bartolomeis, C. Tomasetti, F. Iasevoli, Update on the Mechanism of Action of Aripiprazole: Translational Insights into Antipsychotic Strategies Beyond Dopamine Receptor Antagonism. *CNS Drugs* **29**, 773-799 (2015).

18. R. Nguyen, Investigating the Roles of Parvalbumin and Cholecystokinin Interneurons of the Ventral Hippocampus and Medial Prefrontal Cortex in Schizophrenia-Related Behaviours. (2018).
19. M. I. Atagun, Brain oscillations in bipolar disorder and lithium-induced changes. *Neuropsychiatr Dis Treat* **12**, 589-601 (2016).
20. P. J. Uhlhaas, W. Singer, Abnormal neural oscillations and synchrony in schizophrenia. *Nat Rev Neurosci* **11**, 100-113 (2010).
21. G. Nase, W. Singer, H. Monyer, A. K. Engel, Features of neuronal synchrony in mouse visual cortex. *J Neurophysiol* **90**, 1115-1123 (2003).
22. K. K. Cho, R. Hoch, A. T. Lee, T. Patel, J. L. Rubenstein, V. S. Sohal, Gamma rhythms link prefrontal interneuron dysfunction with cognitive inflexibility in Dlx5/6(+/-) mice. *Neuron* **85**, 1332-1343 (2015).
23. A. R. Bialas, J. Presumey, A. Das, C. E. van der Poel, P. H. Lapchak, L. Mesin, G. Victora, G. C. Tsokos, C. Mawrin, R. Herbst, M. C. Carroll, Microglia-dependent synapse loss in type I interferon-mediated lupus. *Nature* **546**, 539-543 (2017).
24. K. E. Linker, M. G. Elabd, P. Tawadrous, M. Cano, K. N. Green, M. A. Wood, F. M. Leslie, Microglial activation increases cocaine self-administration following adolescent nicotine exposure. *Nat Commun* **11**, 306 (2020).
25. M. P. Wautier, O. Chappey, S. Corda, D. M. Stern, A. M. Schmidt, J. L. Wautier, Activation of NADPH oxidase by AGE links oxidant stress to altered gene expression via RAGE. *Am J Physiol Endocrinol Metab* **280**, E685-694 (2001).
26. R. Suzuki, S. Arata, S. Nakajo, K. Ikenaka, S. Kikuyama, S. Shioda, Expression of the receptor for pituitary adenylate cyclase-activating polypeptide (PAC1-R) in reactive astrocytes. *Brain Res Mol Brain Res* **115**, 10-20 (2003).
27. R. Suzuki, J. Watanabe, S. Arata, H. Funahashi, S. Kikuyama, S. Shioda, A transgenic mouse model for the detailed morphological study of astrocytes. *Neurosci Res* **47**, 451-454 (2003).
28. A. Das, G. C. t. Wallace, C. Holmes, M. L. McDowell, J. A. Smith, J. D. Marshall, L. Bonilha, J. C. Edwards, S. S. Glazier, S. K. Ray, N. L. Banik, Hippocampal tissue of patients with refractory temporal lobe epilepsy is

associated with astrocyte activation, inflammation, and altered expression of channels and receptors. *Neuroscience* **220**, 237-246 (2012).

29. D. D. Mao, W. Y. Yang, Y. Li, J. W. Lin, S. Y. Gao, Y. R. Wang, H. Y. Hu, Effect of Qingxin Kaiqiao Fang on Hippocampus mRNA Expression of the Inflammation-Related Genes IL-1beta, GFAP, and Abeta in an Alzheimer's Disease Rat Model. *Evid Based Complement Alternat Med* **2018**, 9267653 (2018).
30. C. García-Cáceres, C. Quarta, L. Varela, Y. Gao, T. Gruber, B. Legutko, M. Jastroch, P. Johansson, J. Ninkovic, C. X. Yi, O. Le Thuc, K. Szigeti-Buck, W. Cai, C. W. Meyer, P. T. Pfluger, A. M. Fernandez, S. Luquet, S. C. Woods, I. Torres-Alemán, C. R. Kahn, M. Götz, T. L. Horvath, M. H. Tschöp, Astrocytic Insulin Signaling Couples Brain Glucose Uptake with Nutrient Availability. *Cell* **166**, 867-880 (2016).
31. J. P. Luyendyk, J. G. Schoenecker, M. J. Flick, The multifaceted role of fibrinogen in tissue injury and inflammation. *Blood* **133**, 511-520 (2019).
32. J. Paul, S. Strickland, J. P. Melchor, Fibrin deposition accelerates neurovascular damage and neuroinflammation in mouse models of Alzheimer's disease. *J Exp Med* **204**, 1999-2008 (2007).
33. M. Nitta, T. Kishimoto, N. Muller, M. Weiser, M. Davidson, J. M. Kane, C. U. Correll, Adjunctive use of nonsteroidal anti-inflammatory drugs for schizophrenia: a meta-analytic investigation of randomized controlled trials. *Schizophr Bull* **39**, 1230-1241 (2013).
34. J. Savitz, S. Preskorn, T. K. Teague, D. Drevets, W. Yates, W. Drevets, Minocycline and aspirin in the treatment of bipolar depression: a protocol for a proof-of-concept, randomised, double-blind, placebo-controlled, 2x2 clinical trial. *BMJ Open* **2**, e000643 (2012).
35. G. de Gaetano, Low-dose aspirin and vitamin E in people at cardiovascular risk: a randomised trial in general practice. Collaborative Group of the Primary Prevention Project. *Lancet* **357**, 89-95 (2001).
36. E. Magen, J. R. Viskoper, J. Mishal, R. Priluk, D. London, C. Yosefy, Effects of low-dose aspirin on blood pressure and endothelial function of treated hypertensive hypercholesterolaemic subjects. *J Hum Hypertens* **19**, 667-673 (2005).

37. A. Sakasai-Sakai, T. Takata, J. I. Takino, M. Takeuchi, Impact of intracellular glyceraldehyde-derived advanced glycation end-products on human hepatocyte cell death. *Sci Rep* **7**, 14282 (2017).
38. J. J. Hwang, A. Johnson, G. Cline, R. Belfort-DeAguiar, D. Snegovskikh, B. Khokhar, C. S. Han, R. S. Sherwin, Fructose levels are markedly elevated in cerebrospinal fluid compared to plasma in pregnant women. *PLoS One* **10**, e0128582 (2015).
39. P. Steullet, J. H. Cabungcal, J. Coyle, M. Didriksen, K. Gill, A. A. Grace, T. K. Hensch, A. S. LaMantia, L. Lindemann, T. M. Maynard, U. Meyer, H. Morishita, P. O'Donnell, M. Puhl, M. Cuenod, K. Q. Do, Oxidative stress-driven parvalbumin interneuron impairment as a common mechanism in models of schizophrenia. *Mol Psychiatry* **22**, 936-943 (2017).
40. O. Kann, The interneuron energy hypothesis: Implications for brain disease. *Neurobiol Dis* **90**, 75-85 (2016).
41. C. L. Beasley, G. P. Reynolds, Parvalbumin-immunoreactive neurons are reduced in the prefrontal cortex of schizophrenics. *Schizophr Res* **24**, 349-355 (1997).
42. T. Hashimoto, D. W. Volk, S. M. Eggan, K. Mirnics, J. N. Pierri, Z. Sun, A. R. Sampson, D. A. Lewis, Gene expression deficits in a subclass of GABA neurons in the prefrontal cortex of subjects with schizophrenia. *J Neurosci* **23**, 6315-6326 (2003).
43. M. Thompson, C. S. Weickert, E. Wyatt, M. J. Webster, Decreased glutamic acid decarboxylase(67) mRNA expression in multiple brain areas of patients with schizophrenia and mood disorders. *J Psychiatr Res* **43**, 970-977 (2009).
44. T. R. Insel, Rethinking schizophrenia. *Nature* **468**, 187-193 (2010).
45. C. Menard, M. L. Pfau, G. E. Hodes, V. Kana, V. X. Wang, S. Bouchard, A. Takahashi, M. E. Flanigan, H. Aleyasin, K. B. LeClair, W. G. Janssen, B. Labonte, E. M. Parise, Z. S. Lorsch, S. A. Golden, M. Heshmati, C. Tamminga, G. Turecki, M. Campbell, Z. A. Fayad, C. Y. Tang, M. Merad, S. J. Russo, Social stress induces neurovascular pathology promoting depression. *Nat Neurosci* **20**, 1752-1760 (2017).
46. W. A. Banks, A. M. Gray, M. A. Erickson, T. S. Salameh, M. Damodarasamy, N. Sheibani, J. S. Meabon, E. E. Wing, Y. Morofuji, D. G. Cook, M. J. Reed, Lipopolysaccharide-induced blood-brain barrier disruption: roles of

cyclooxygenase, oxidative stress, neuroinflammation, and elements of the neurovascular unit. *J Neuroinflammation* **12**, 223 (2015).

47. D. Ben-Nathan, S. Lustig, H. D. Danenberg, Stress-induced neuroinvasiveness of a neurovirulent noninvasive Sindbis virus in cold or isolation subjected mice. *Life Sci* **48**, 1493-1500 (1991).
48. D. Koshiyama, M. Fukunaga, N. Okada, K. Morita, K. Nemoto, K. Usui, H. Yamamori, Y. Yasuda, M. Fujimoto, N. Kudo, H. Azechi, Y. Watanabe, N. Hashimoto, H. Narita, I. Kusumi, K. Ohi, T. Shimada, Y. Kataoka, M. Yamamoto, N. Ozaki, G. Okada, Y. Okamoto, K. Harada, K. Matsuo, H. Yamasue, O. Abe, R. Hashimoto, T. Takahashi, T. Hori, M. Nakataki, T. Onitsuka, L. Holleran, N. Jahanshad, T. G. M. van Erp, J. Turner, G. Donohoe, P. M. Thompson, K. Kasai, R. Hashimoto, White matter microstructural alterations across four major psychiatric disorders: mega-analysis study in 2937 individuals. *Mol Psychiatry*, (2019).
49. V. Nascimento-Silva, M. A. Arruda, C. Barja-Fidalgo, I. M. Fierro, Aspirin-triggered lipoxin A4 blocks reactive oxygen species generation in endothelial cells: a novel antioxidative mechanism. *Thromb Haemost* **97**, 88-98 (2007).
50. M. S. Dzeshka, A. Shantsila, G. Y. Lip, Effects of Aspirin on Endothelial Function and Hypertension. *Curr Hypertens Rep* **18**, 83 (2016).
51. C. M. Sena, P. Matafome, J. Crisostomo, L. Rodrigues, R. Fernandes, P. Pereira, R. M. Seica, Methylglyoxal promotes oxidative stress and endothelial dysfunction. *Pharmacol Res* **65**, 497-506 (2012).
52. W. Cai, J. C. He, L. Zhu, C. Lu, H. Vlassara, Advanced glycation end product (AGE) receptor 1 suppresses cell oxidant stress and activation signaling via EGF receptor. *Proc Natl Acad Sci U S A* **103**, 13801-13806 (2006).
53. E. Kim, Z. Keskey, M. Kang, C. Kitchen, W. E. Bentley, S. Chen, D. L. Kelly, G. F. Payne, Validation of oxidative stress assay for schizophrenia. *Schizophr Res* **212**, 126-133 (2019).
54. K. Toriumi, S. Berto, S. Koike, N. Usui, T. Dan, K. Suzuki, M. Miyashita, Y. Horiuchi, A. Yoshikawa, Y. Sugaya, T. Watanabe, M. Asakura, M. Kano, Y. Ogasawara, T. Miyata, M. Itokawa, G. Konopka, M. Arai, Impairment of methylglyoxal detoxification systems causes mitochondrial dysfunction and schizophrenia-like behavioral deficits. *bioRxiv*, (2020).

55. A. V. Kalueff, A. M. Stewart, C. Song, K. C. Berridge, A. M. Graybiel, J. C. Fentress, Neurobiology of rodent self-grooming and its value for translational neuroscience. *Nat Rev Neurosci* **17**, 45-59 (2016).

56. P. Jirkof, Burrowing and nest building behavior as indicators of well-being in mice. *J Neurosci Methods* **234**, 139-146 (2014).

57. C. S. Pedersen, D. B. Sorensen, A. I. Parachikova, N. Plath, PCP-induced deficits in murine nest building activity: employment of an ethological rodent behavior to mimic negative-like symptoms of schizophrenia. *Behav Brain Res* **273**, 63-72 (2014).

58. A. Forsingdal, K. Fejgin, V. Nielsen, T. Werge, J. Nielsen, 15q13.3 homozygous knockout mouse model display epilepsy-, autism- and schizophrenia-related phenotypes. *Transl Psychiatry* **6**, e860 (2016).

59. A. Ennaceur, J. Delacour, A new one-trial test for neurobiological studies of memory in rats. 1: Behavioral data. *Behav Brain Res* **31**, 47-59 (1988).

60. J. L. Silverman, S. S. Tolu, C. L. Barkan, J. N. Crawley, Repetitive self-grooming behavior in the BTBR mouse model of autism is blocked by the mGluR5 antagonist MPEP. *Neuropsychopharmacology* **35**, 976-989 (2010).

61. L. A. Tellez, W. Han, X. Zhang, T. L. Ferreira, I. O. Perez, S. J. Shammah-Lagnado, A. N. van den Pol, I. E. de Araujo, Separate circuitries encode the hedonic and nutritional values of sugar. *Nat Neurosci* **19**, 465-470 (2016).

62. W. T. Golde, P. Gollobin, L. L. Rodriguez, A rapid, simple, and humane method for submandibular bleeding of mice using a lancet. *Lab Anim (NY)* **34**, 39-43 (2005).

Figure 1

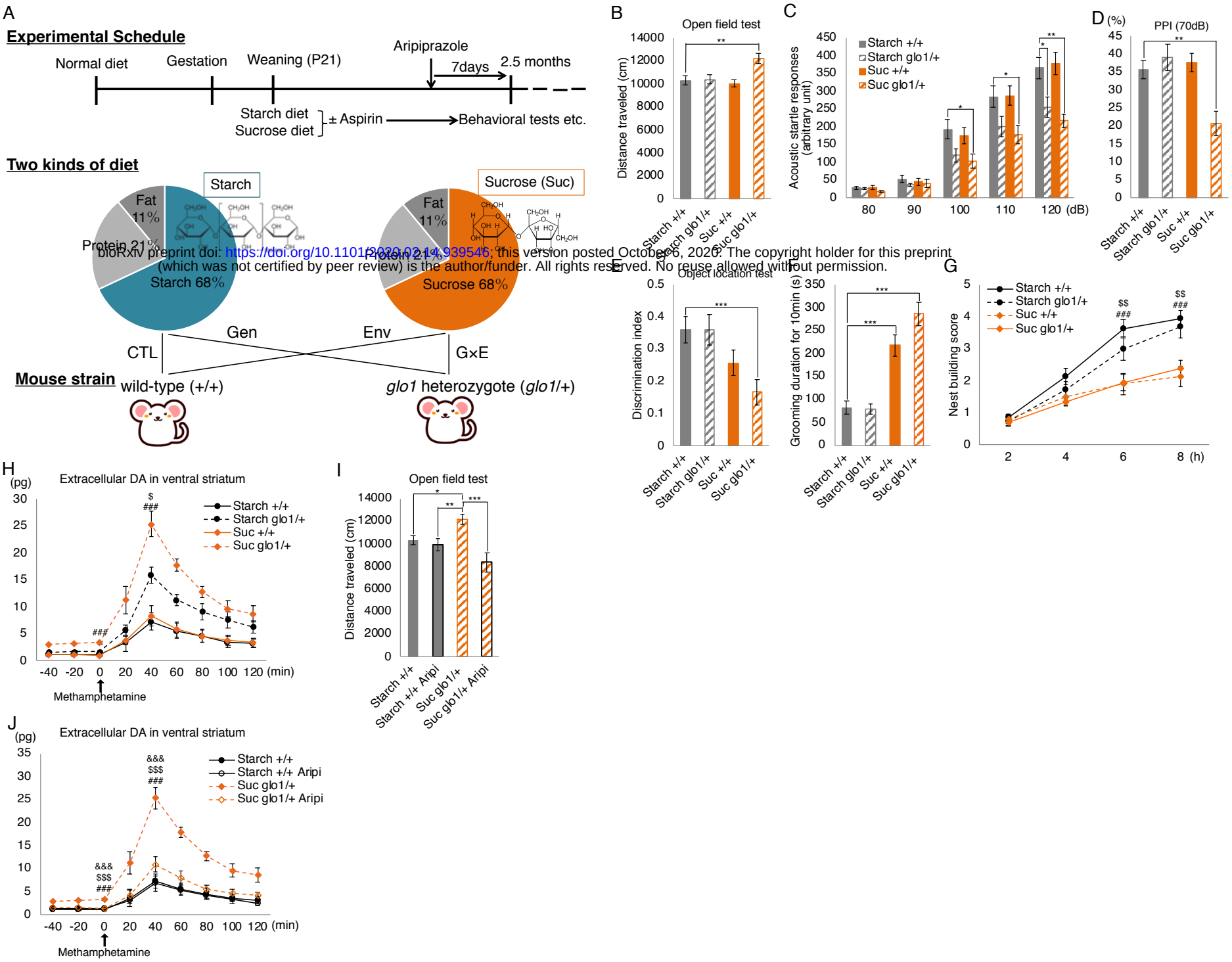

Fig. 1 Generation of G × E model mice and analyses of psychosis-related phenotypes.
(**A**) Timeline of the experiments. After weaning (P21), wild-type (WT) and *Glo1* heterozygous mutant mice were fed either a starch diet (control) or a sucrose diet (experimental). Diets were equal in total calories and proportions of calories from carbohydrates, lipids, and proteins. The behavioral test battery was administered starting at 2.5 months of age (upper panel). Middle panel: Macronutrient composition of the two diets. We used *Glo1* heterozygous mice to mimic patients with psychiatric disorders who exhibit decreased GLO1 activity or expression, whereas the high-sucrose intake was used as the environmental risk factor (bottom panel). We investigated four groups of mice: WT, starch-fed mice (Starch +/+); *Glo1* heterozygous, starch-fed mice (Starch *glo1*/+); WT, sucrose-fed mice (Suc +/+); and *Glo1* heterozygous, sucrose-fed mice (Suc *glo1*/+). (**B–G**) Behavioral analyses of the four groups of mice (n = 18–23 mice per group). (**B**) Spontaneous locomotor activity in the open-field test. (**C**) Acoustic startle responses. (**D**) Pre-pulse inhibition (PPI) using a 70 dB pre-pulse. (**E**) Object location test to evaluate working memory. (**F**) Duration of self-grooming in the home cage. (**G**) Quantification of nest building skills over 8 h. Post hoc Dunnett's multiple comparisons test among groups at specific time point indicated, ###$p < 0.001$ for Suc *glo1*/+ vs. Ctrl (Starch +/+), $$$p < 0.01$ for Suc +/+ vs. Ctrl (Starch +/+). (**H, J**) Extracellular dopamine concentration in the nucleus accumbens (NAc) measured at 20 min intervals using an *in vivo* microdialysis system in the presence or absence of aripiprazole (Aripi). Methamphetamine (1.25 mg/kg) was administered via an intraperitoneal (i.p.) injection at time 0 (arrow) (n = 6–11 mice per group). (**H**) Post hoc Dunnett's multiple comparisons test of groups is performed only at specific time points (0min and 40min), ###$p < 0.001$ for Suc *glo1*/+ vs. Ctrl (Starch +/+), $$p < 0.05$ for Starch *glo1*/+ vs. Ctrl (Starch +/+). (**I**) Effects of Aripi treatment on locomotor activity (n = 12–18 mice per group). (**J**) Post hoc Bonferroni's multiple comparisons test of groups is performed only at specific time points (0min and 40min), ###$p < 0.001$ for Suc *glo1*/+ vs. Starch +/+, $$$$p < 0.001$ for Suc *glo1*/+ vs. Starch +/+ Aripi, &&&$p < 0.001$ for Suc *glo1*/+ vs. Suc *glo1*/+ Aripi. (B-H) Starch +/+ group was used as a control for post hoc Dunnett's test.

Figure 2

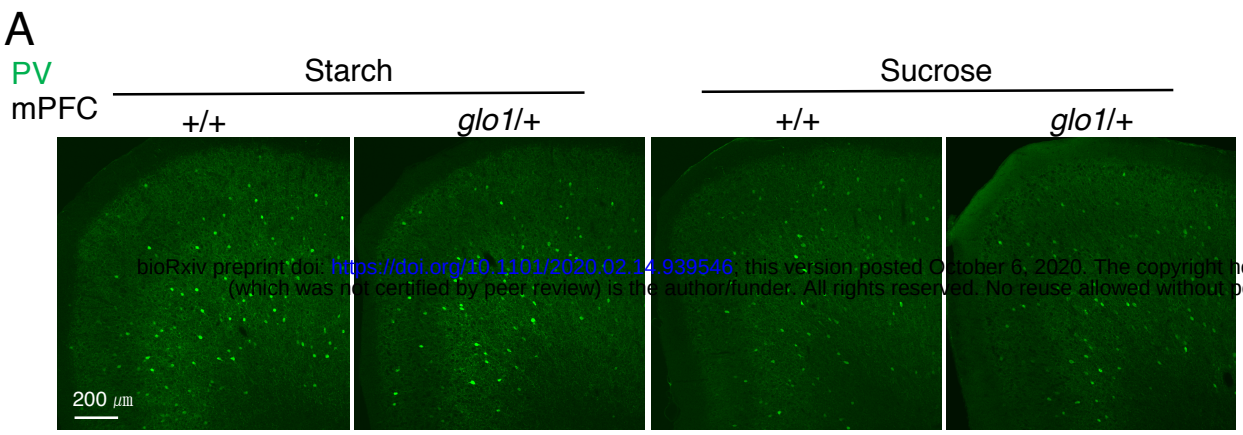

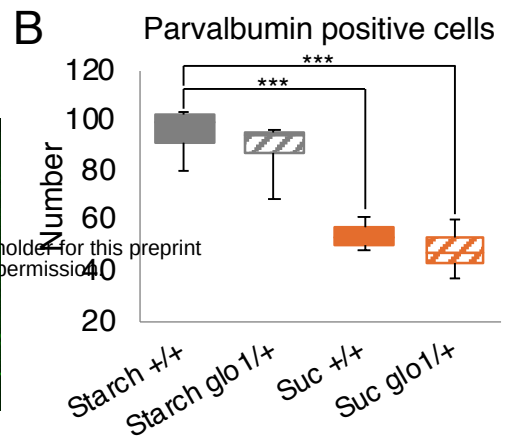

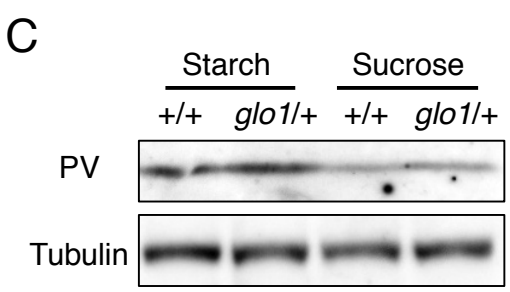

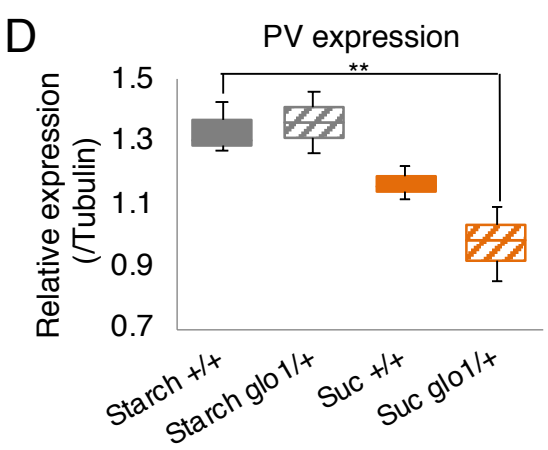

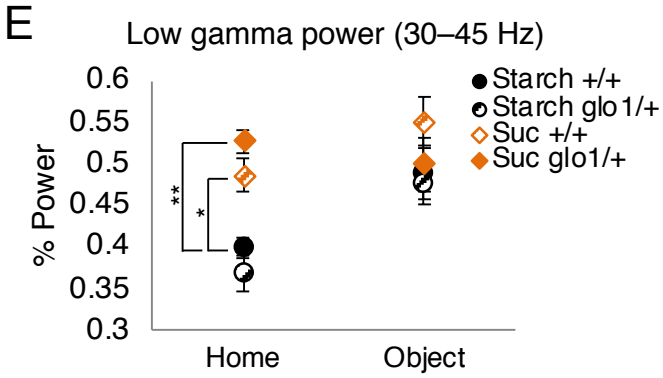

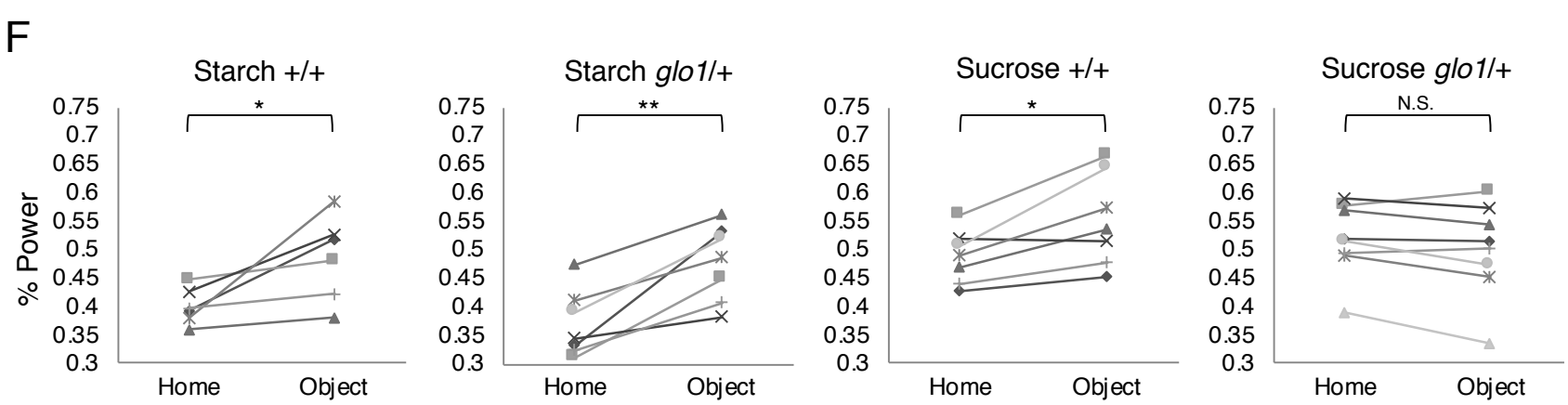

Fig. 2 Parvalbumin-positive interneuron dysfunction in G × E mice.
(**A**) Immunohistochemistry of parvalbumin (PV) in medial prefrontal cortex (mPFC). (**B**) Number of PV-positive cells in the mPFC (n = 4 mice per group). (**C**) Western blot analysis of PV protein expression using tubulin as the internal control. (**D**) Densitometric analysis of PV protein expression: to quantify the expression, PV band intensities were divided by corresponding tubulin band intensities (n = 3 mice per group). (**E**) Average gamma band power in the home cage and during novel object recognition in the open field (n = 7-8 mice per group). (**F**) Changes in gamma band power from the home cage to the novel object phase in individual mice (n = 7-8 mice per group). Each *p* value indicates the result of repeated measures ANOVA. The effect of changes in gamma power at Starch +/+ ($F1, 5 = 8.29$, $p = 0.035$), at Starch *glo1*/+ ($F1, 6 = 29.75$, $p = 0.0016$), at Sucrose +/+ ($F1, 6 = 12.04$, $p = 0.013$), at Sucrose *glo1*/+ ($F1, 7 = 4.038$, $p = 0.084$). (B, D, H) Starch +/+ group was used as a control for post hoc Dunnett's test.

Figure 3

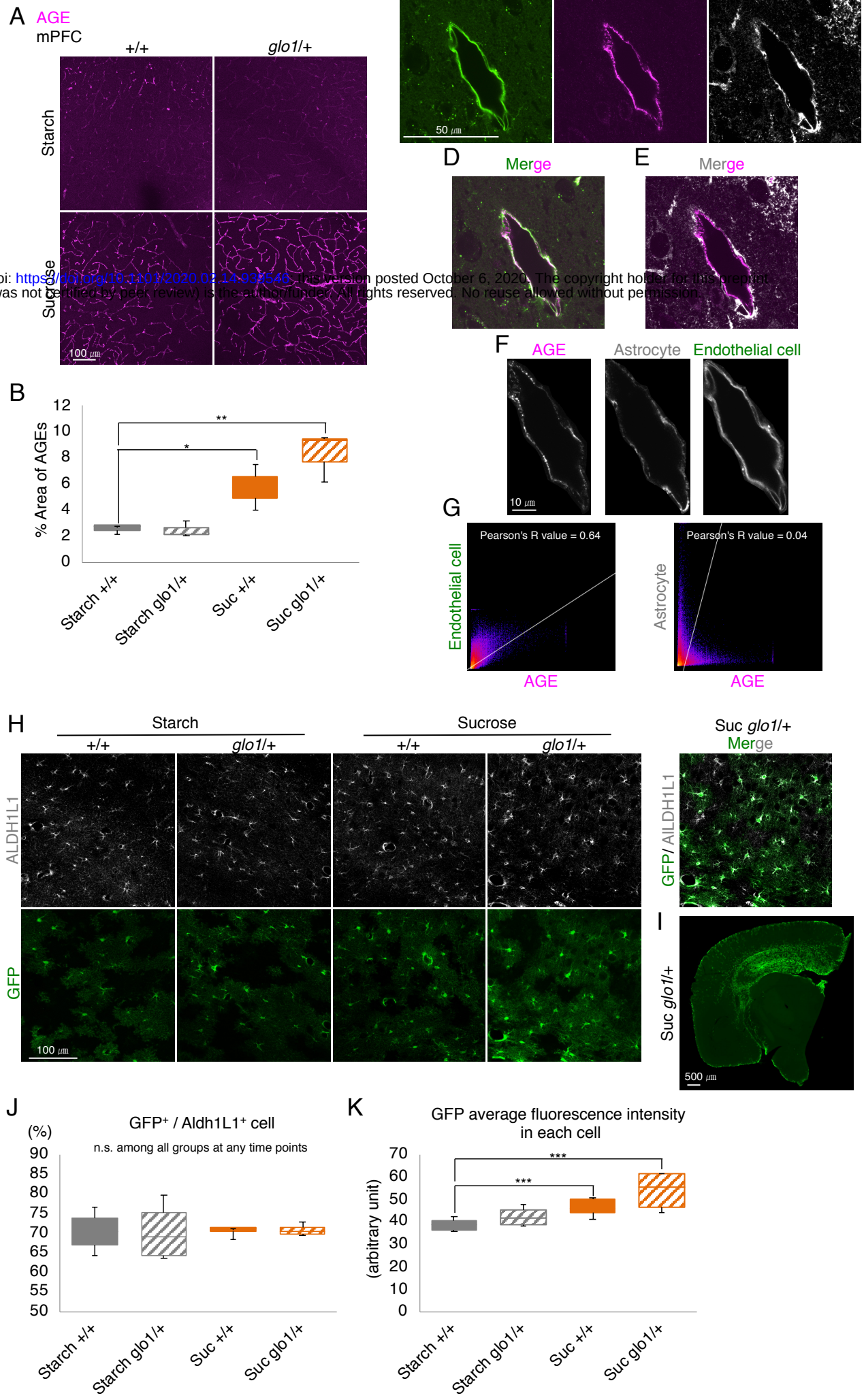

Fig. 3 AGE accumulation in the neurovascular endothelium and pre-inflammatory status of astrocytes in G × E mice. (**A**) Images of AGE immunohistochemistry in the medial prefrontal cortex. (**B**) Measurement of the area covered by AGE immunoreactivity. The mean intensity of the AGE-immunopositive area of the entire image was measured in each section (n = 3 mice per group). (**C–E**) Immunohistochemical images showing colocalization of the endothelial cell marker tomato lectin with the astrocyte marker ALDH1L1 or AGEs. (**F**) Enlarged version of images in (**C**) presenting the region subjected to colocalization analysis. (**G**) 2D intensity histogram of the two indicated channels for identifying the colocalization of AGE with ALDH1L1 or tomato lectin and interpreting the strength of the relationship based on R as follows: $R \geq 0.7$, strong; $0.7 > R \geq 0.4$, moderate; $0.4 > R \geq 0.2$, weak; and $R < 0.2$, none or very weak. (**H**) Immunohistological images of GFP-positive astrocytes and ALDH1L1in the hippocampal CA1 region and merged image of GFP with ALDH1L1. (**I**) Percentage of GFP-positive cells per total ALDH1L1-positive cells in each image presented in (**H**). (**K**) Mean fluorescent GFP intensities of 10 randomly selected cells per image in (**H**) (from four independent mice). (**B, J ,K**) Starch +/+ group was used as a control for post hoc Dunnett's test.

Figure 4

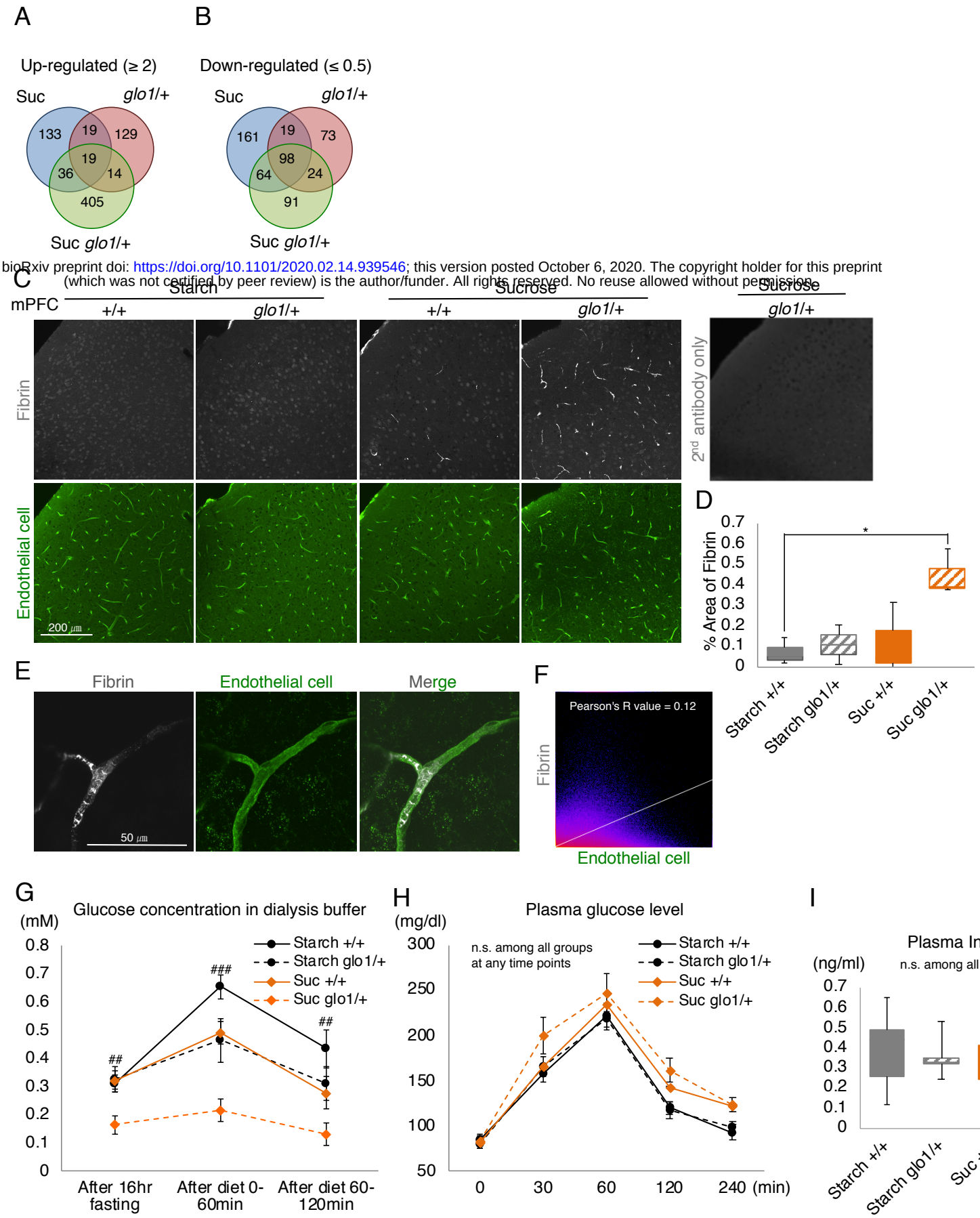

Fig. 4 Angiopathy and impaired glucose transport in G × E mice.
(**A, B**) Venn graph showing the overlap in prefrontal cortex genes exhibiting a >2-fold (**A**) or <0.5-fold (**B**) expression change compared with the CTL group (n = 3 mice per group). (**C**) Immunohistochemical images of fibrin and the endothelial cell marker tomato lectin. (**D**) Measurement of the area covered by fibrin immunoexpression in (**C**). The mean intensity of the fibrin-immunopositive area of the entire image was measured for each section (n = 4 mice per group). (**E**) Immunohistochemical images of fibrin and tomato lectin. (**F**) 2D intensity histogram of the two indicated channels using the left and middle panels in (**E**) for identifying the fibrin colocalization with tomato lectin and interpreting the strength of the relationship based on R as follows: R ≥ 0.7, strong; 0.7 > R ≥ 0.4, moderate; 0.4 > R ≥ 0.2, weak; and R < 0.2, none or very weak. (**G**) Extracellular concentrations of glucose in the dialysis buffer at each time point [1 h collection after 16 h of fasting, 0–1 h after eating 0.05 g of carbohydrate (starch or sucrose), and 1–2 h after eating 0.05 g of carbohydrate (starch or sucrose) (n = 5-6 mice per group)]. Post hoc Dunnett's multiple comparisons test of groups at specific time points, ###p < 0.001, ##p < 0.01 for Suc *glo1*/+ vs. Ctrl (Starch +/+). (**H**) Plasma glucose concentrations in wild-type (WT) and *Glo1* heterozygous mice (n = 6-7 mice per group). The first measurement was performed after 16 h of fasting, and the second blood collection was performed 30 min after eating 0.05 g of carbohydrate. No significant differences were observed among groups. (**I**) Fasting plasma insulin levels in WT and *Glo1* heterozygous mice. No significant differences were observed among groups (n = 5-6 mice per group). (**D, G-I**) Starch +/+ group was used as a control for post hoc Dunnett's test.

Figure 5

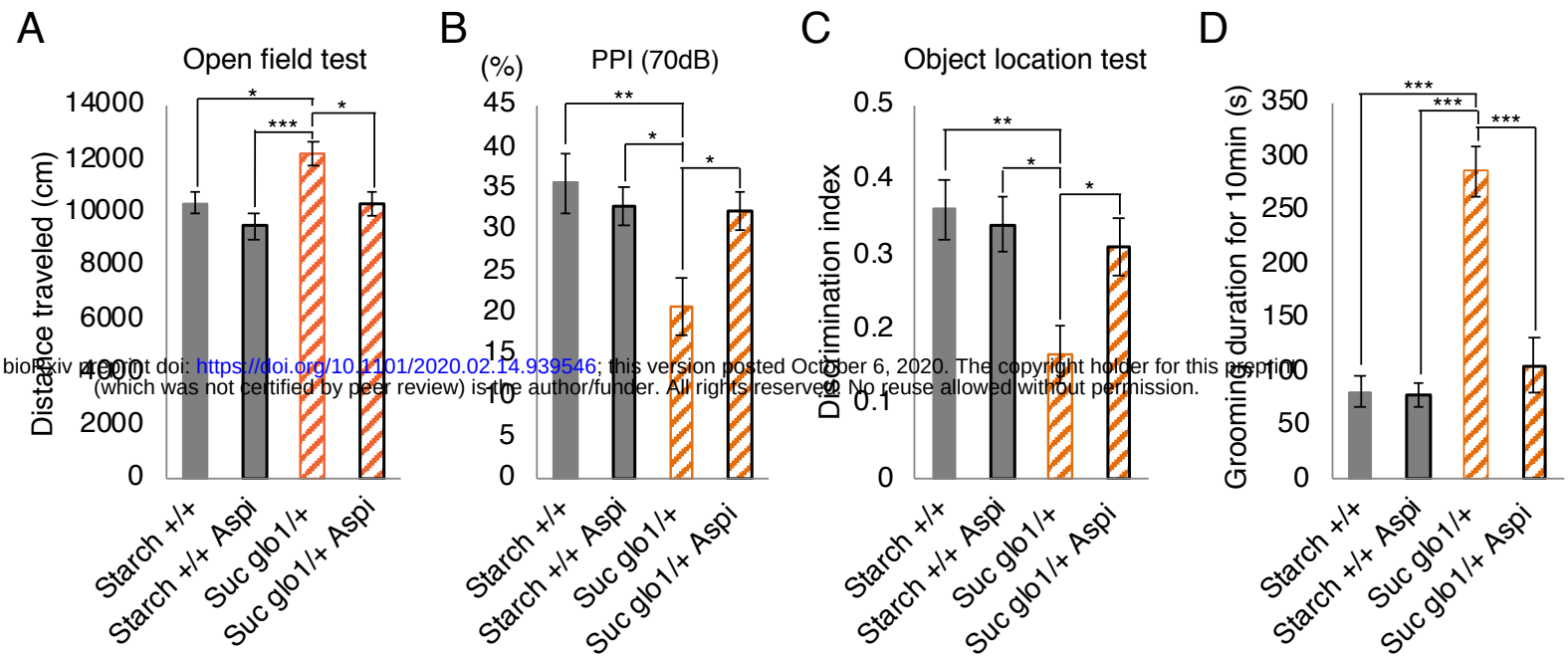

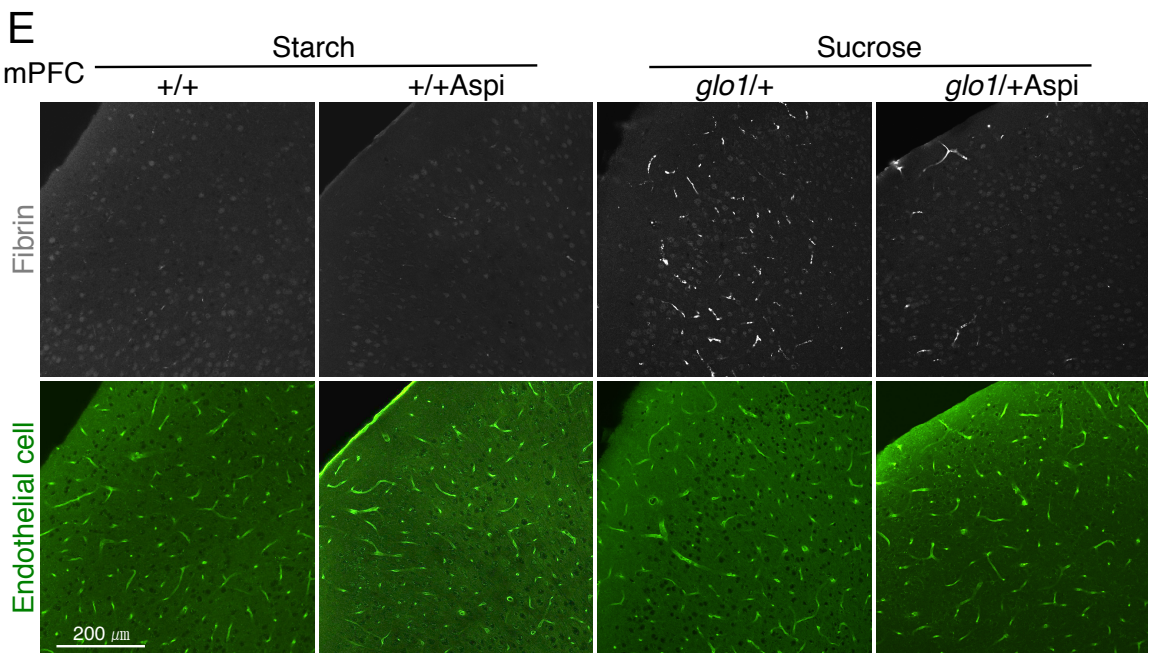

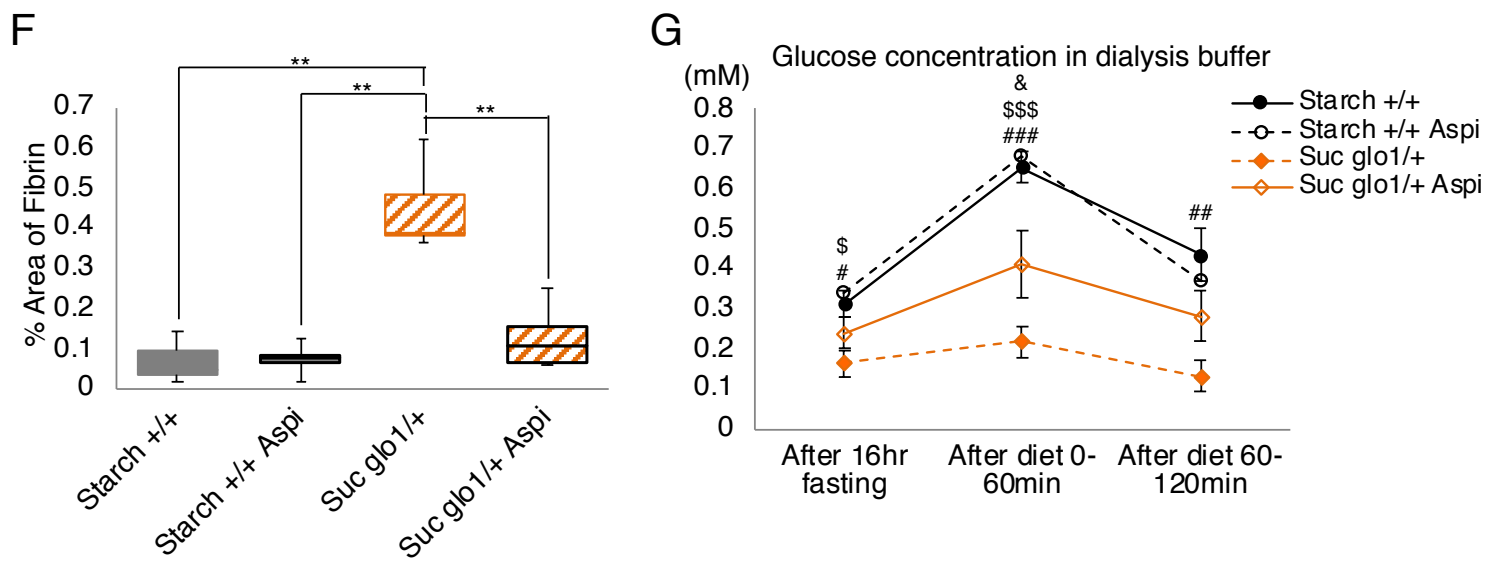

Fig. 5 Protective effects of low-dose aspirin in G × E mice.
(**A–D**) Results of behavioral tests performed to evaluate the effects of aspirin treatment (n = 12–21 mice per group). (**A**) Quantifications of spontaneous locomotor activity in the open field. (**B**) Pre-pulse inhibition at 70 dB. (**C**) Object location test of working memory. (**D**) Quantification of nest building skills over 8 h. (**E**) Immunohistochemical images of fibrin and the endothelial cell marker tomato lectin. (**F**) Measurement of the area covered by fibrin immunoexpression in (**E**). The mean intensity of the fibrin-immunopositive area of the entire image was measured for each section (n = 3 mice per group). (**G**) Extracellular concentrations of glucose in the dialysis buffer at each time point (1 h collection after 16 h of fasting, 0–1 h after eating 0.05 g of carbohydrate, and 1–2 h after eating 0.05 g of carbohydrate) (n = 4–6 mice per group). Post hoc Tukey's multiple comparisons test of groups at specific time points, ###$p < 0.001$, ##$p < 0.01$, #$p < 0.05$ for Starch +/+ vs. Suc *glo1*/+, \$\$\$$p < 0.001$, \$$p < 0.05$ for Starch +/+ Aspi vs. Suc *glo1*/+, &$p < 0.05$ for Starch +/+ vs. Suc *glo1*/+ Asp.

Figure 6

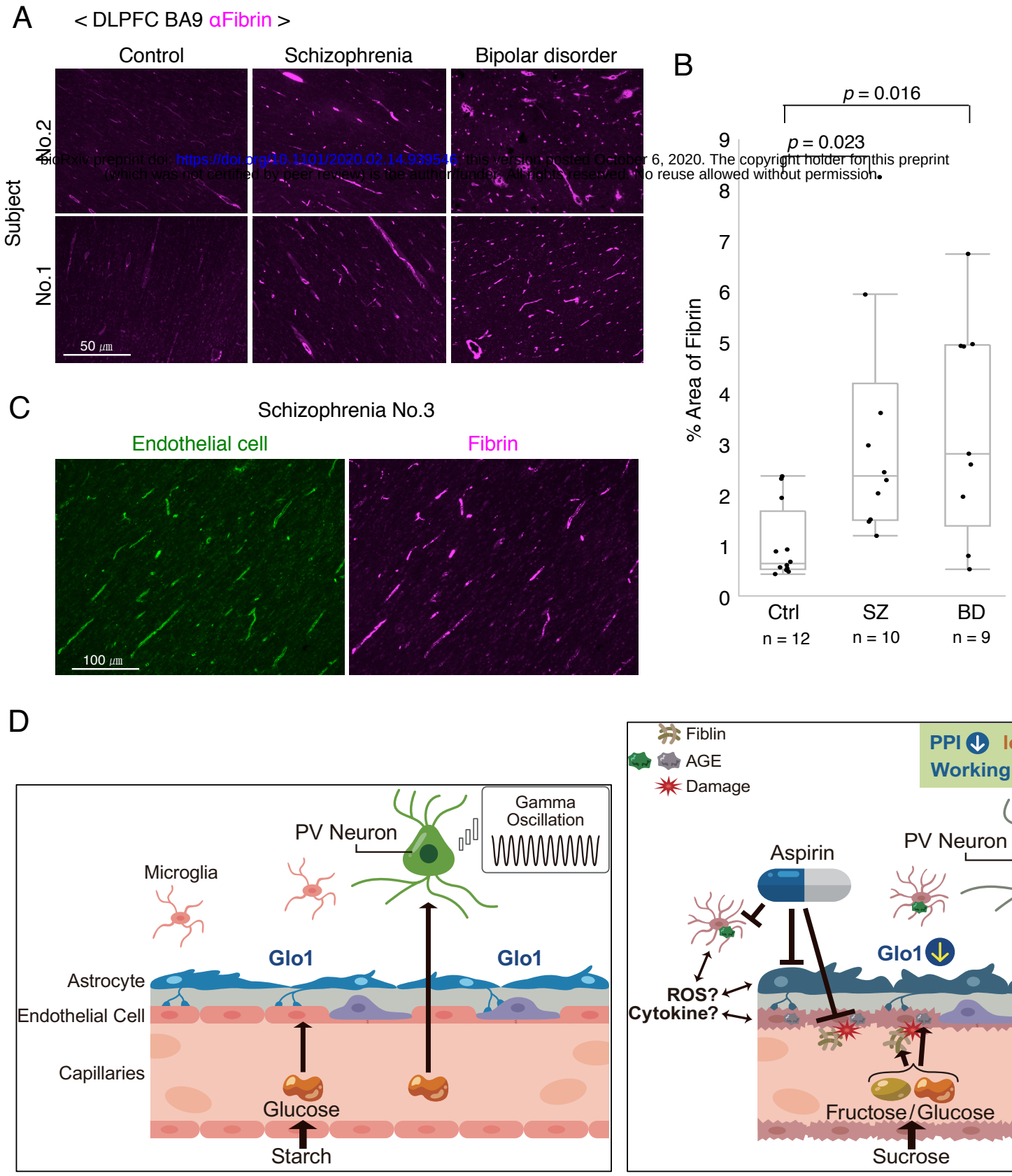

Fig. 6 Angiopathy in postmortem brains from individuals with psychiatric disorders.
(**A**) Representative immunohistochemical images of fibrin in the BA9 region of postmortem brains from controls and patients with schizophrenia (SZ) or bipolar disorder (BD). (**B**) Measurement of the area covered by fibrin immunoexpression in (**A**). The mean intensity of the fibrin-immunopositive area of the entire image was measured for each section. (**C**) Representative immunohistochemical images of fibrin (magenta) and the endothelial cell marker tomato lectin (green) in postmortem brains from a patient with SZ. Fibrin-positive areas are merged with areas of vascular endothelial cell marker expression. (**D**) Diagrams describing the hypothesis proposed to explain functional and behavioral abnormalities in CTL mice (left) and G × E mice (right) (see Discussion for details).